

Higher vortexability: zero field realization of higher Landau levels

Manato Fujimoto,^{1,2} Daniel E. Parker,^{3,4} Junkai Dong,¹ Eslam Khalaf,¹ Ashvin Vishwanath,¹ and Patrick Ledwith¹

¹*Department of Physics, Harvard University, Cambridge, Massachusetts 02138, USA*

²*Department of Applied Physics, The University of Tokyo, Hongo, Tokyo, 113-8656, Japan*

³*Department of Physics, University of California at Berkeley, Berkeley, CA 94720, USA*

⁴*Department of Physics, University of California at San Diego, La Jolla, California 92093, USA*

(Dated: March 5, 2024)

The rise of moiré materials has led to experimental realizations of integer and fractional Chern insulators in small or vanishing magnetic fields. At the same time, a set of minimal conditions sufficient to guarantee an Abelian fractional state in a flat band were identified, namely “ideal” or “vortexable” quantum geometry. Such vortexable bands share essential features with the lowest Landau level, while excluding the need for more fine-tuned aspects such as flat Berry curvature. A natural and important generalization is to ask if such conditions can be extended to capture the quantum geometry of higher Landau levels, particularly the first (1LL), where non-Abelian states at $\nu = 1/2, 2/5$ are known to be competitive. The possibility of realizing these states at zero magnetic field, and perhaps even more exotic ones, could become a reality if we could identify the essential structure of the 1LL in Chern bands. In this work, we introduce a precise definition of 1LL quantum geometry, along with a figure of merit that measures how closely a given band approaches the 1LL. We apply the definition to identify two models with 1LL structure — a toy model of double bilayer twisted graphene and a more realistic model of strained Bernal graphene.

Fractional quantum Hall (FQH) states, whose quasiparticles have fractional electronic charge and anyonic particle statistics, constitute a stunning example of emergent behavior in condensed matter physics [1]. Traditionally, these states have been studied in Landau levels (LLs) in the regime of large external magnetic fields and milli-Kelvin temperatures. Fractional Chern Insulators (FCIs) [2–10] realize FQH physics in Chern bands, which do not require a magnetic field and can potentially form at much higher temperatures [11–17]. While first observed in Harper-Hofstadter bands [11], they were recently observed in the Chern bands of twisted bilayer graphene with the help of a small magnetic field [12]. Not only does the field reduce the bandwidth [18], but it was also argued to improve the wavefunctions of the Chern band, pushing them to an “ideal” [19] or “vortexable” [20] limit where the band becomes directly analogous to the lowest Landau level [21–29]. More recently, Abelian fractional Chern insulators at zero magnetic field, dubbed fractional quantum anomalous Hall (FQAH) states, were observed in twisted MoTe₂ [13–16], following theoretical works showcasing small bandwidths and numerical works finding FCI ground states [30–42], and also in pentalayer graphene [17, 43–48]. As these zero field devices improve, they will likely run the gamut of Abelian topological orders found in the lowest Landau level.

To date, experimental realizations of non-Abelian topological order are the almost-exclusive province of the first Landau level at half filling. Namely, the $\nu = 5/2$ state of GaAs (half-filling of the first spinful Landau level) [49–51], and half-filling of 1LLs in Bernal graphene [52–56] realize a Pfaffian-type state with non-Abelian particle statistics [57]. Also, experiments [58] at $\nu = 2 + 2/5$ have seen an unusually stable plateau which is suspected of being a non-Abelian phase harboring Fibonacci anyons [59], a scenario that has received numer-

ical support [59, 60]. These states are not only of immense theoretical interest, but of potential practical importance as a platform for topological quantum computation [61, 62] that is innately protected from decoherence. Since the effective magnetic fields in Chern bands can greatly exceed laboratory ones, this direction to achieving non-Abelian states holds the potential to realize them with elevated energy scales. This raises the question — are there Chern bands at zero magnetic field analogous to the *first* Landau level?

In this work we answer this question by providing a precise definition of what it means for a band to be similar to the first LL. Our definition makes use of “vortexability” applied to multi-band systems, and requires two bands. A Chern band with first LL structure has a related band that acts as the zeroth LL. Vortex attachment applied to both bands produces *exact* Jain-like [63] ground states in the limit of short-range repulsive interactions, without the need for further projection. We argue that single-band definitions, such as those based on the Fubini-Study metric used for the LLL case [21], cannot capture first Landau level structure. Below we motivate and explicate our definition, then provide two concrete examples in zero-field superlattice systems, one exact and the other approximate but physically realistic. Our construction is readily extendable to higher Chern bands, by forming $(n + 1)$ Chern band complexes to capture the geometry of the ‘*n*th’ Landau level.

Quantum Geometry Review— We begin by reviewing the point of view that has recently emerged on “LLL band geometry,” through *ideal*, or *vortexable*, Chern bands [19, 20, 23–29, 64–67]. These names refer to the following equivalent criteria. (i) The bands are vortexable [20]: $z\psi = Pz\psi$, where P is the projector onto the band(s) of interest, $\psi = P\psi$ is a wavefunction in those bands, and $z = x + iy$ is the vor-

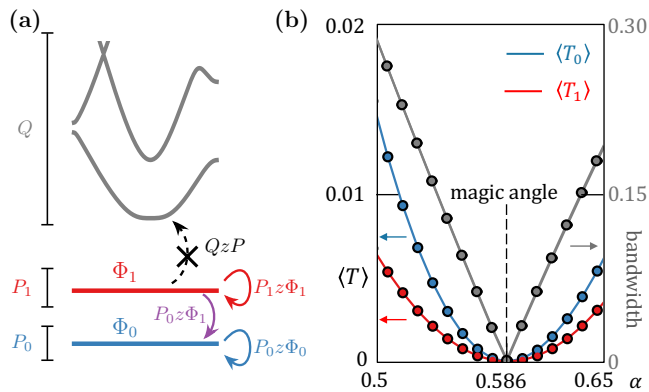


FIG. 1. (a) Cartoon depicting the first two parts of the definition of a first vortexable band, with band projector P_1 . (b) Bandstructure of a toy model (2) that realizes a first vortexable band at its magic angle. The gray line represents the bandwidth of the set of four low-energy bands as a function of α for $\gamma_1 = 1$. The bandwidth becomes zero at the magic angle of TBG, $\alpha = 0.586$. The blue and red lines are the averaged overlaps $\langle T_n \rangle_{BZ}$ for $n = 0$ and $n = 1$, respectively.

tex function. (ii) The bands satisfy the trace condition $\text{tr } g(\mathbf{k}) = \Omega(\mathbf{k})$ [68, 69], where $g_{\mu\nu}(\mathbf{k})$ is the Fubini-Study metric and $\Omega(\mathbf{k})$ is the Berry curvature. (iii) The cell-periodic states $u_{\mathbf{k}a}(\mathbf{r}) = e^{-i\mathbf{k}\cdot\mathbf{r}}\psi_{\mathbf{k}a}(\mathbf{r})$ can be written as holomorphic functions of $k = k_x + ik_y$ up to orthonormality (here “ a ” is a band index) [22, 26, 70]. More general vortex functions [20] with correspondingly generalized trace conditions (suitable for other unit cell embeddings [71]) are immediate but avoided here for concision. For zero dispersion vortexable bands, Laughlin-like trial states constructed by attaching vortices (i.e. Jastrow factors) $\prod_{i<j}(z_i - z_j)^{2m}$ to integer filling states are exact many-body ground states in the limit of short range repulsive interactions [20, 23, 72].

Wavefunctions for $C = 1$ ideal bands have the form [19, 23]

$$\psi(\mathbf{r}) = f(z)\mathcal{N}_0(\mathbf{r}); \quad \mathcal{N}_0^l(\mathbf{r}) = e^{-K(\mathbf{r})}\zeta^l(\mathbf{r}) \quad (1)$$

where $f(z)$ is holomorphic, $\zeta^l(\mathbf{r})$ is a orbital-space spinor (with layer index l , e.g.), and $\phi(\mathbf{r}) = f(z)e^{-K(\mathbf{r})}$ is a zero mode of a Dirac particle in the inhomogeneous magnetic field $B(\mathbf{r}) = \nabla^2 \text{Re } K(\mathbf{r})$. Due to its normalization $\sum_l |\zeta^l(\mathbf{r})|^2 = 1$ the spinor part does not influence the energy of the band under density-density interactions, and can thus be largely ignored for our purposes. The class of $C = 1$ vortexable bands therefore has the same analytic structure as the LLL in an inhomogeneous magnetic field and metric that breaks continuous translation symmetry [23, 66]. Vortexability is thus a sufficient condition for a Chern band to be “analogous to the LLL”.

First Landau Levels Are Diverse— To extend the success of ideal bands to the first Landau level, one could imagine imposing band geometric criteria to mimic a 1LL

features. For example, the first Landau level of a $p^2/2m$ particle has $\text{tr } g = 3\Omega$ [25]. However, this and other approaches fail to capture the wide spectrum of “first Landau levels” in multilayer graphene. To wit, we recall Bernal graphene at $B > 0$:

$$H_{BG} = \begin{pmatrix} 0 & D_1^\dagger \\ D_1 & 0 \end{pmatrix}, \quad D_1 = \begin{pmatrix} D_0 & \gamma_1 \\ 0 & D_0 \end{pmatrix}, \quad (2)$$

written in the chiral basis ($|A, 1\rangle, |A, 2\rangle, |B, 1\rangle, |B, 2\rangle$). Here $D_0 = 2v(-i\bar{\partial}_z - \bar{A}_z) = \sqrt{2}v\ell_B^{-1}\hat{a}$ is proportional to the annihilation operator and γ_1 is the interlayer coupling. There are two bands of zero modes; $\ker D_1$ is spanned by

$$\Phi_0 = \begin{pmatrix} \psi_0 \\ 0 \end{pmatrix}, \quad \Phi_1 = \begin{pmatrix} v^{-1}\ell_B\gamma_1\hat{a}^\dagger\psi_0 \\ -\sqrt{2}\psi_0 \end{pmatrix}, \quad (3)$$

forming a zeroth and first LL respectively, where $\psi_0(\mathbf{r}) = f(z)e^{-|z|^2/4\ell_B^2}$ in symmetric gauge with $f(z)$ holomorphic.

Direct computation shows that, as γ_1 varies from 0 to ∞ , the ratio $\text{tr } g^{(1)}/\Omega^{(1)}$ of band Φ_1 varies continuously from 1 to 3. However, the wavefunctions have a similar analytic structure throughout. Even if one insists the first Landau level corresponds only to the $\gamma_1 \rightarrow \infty$ limit, with $\text{tr } g^{(1)} = 3\Omega^{(1)}$, the condition $\text{tr } g = 3\Omega$ is also satisfied by the second Landau level of trilayer graphene for a particular value of $v^{-1}\ell_B\gamma_1$. The single-band Berry curvature and quantum metric therefore appear insufficient to specify a first Landau level structure.

A clue for a more encompassing definition comes from the observation that, while the band described by Φ_1 is not vortexable, the two-band system (Φ_0, Φ_1) is, for any γ_1 . To see this, note $[D_1, z] = 0$ so that if Φ is a zero mode, then so is $z\Phi$, fulfilling criteria (i) above. Alternatively, using $z\hat{a}^\dagger = \hat{a}^\dagger z + \ell_B/\sqrt{2}$ yields

$$z\Phi_1 = \Phi_1' + (\ell_B/\sqrt{2})\Phi_0, \quad z\Phi_0 = \Phi_0' \quad (4)$$

where Φ_i' has $f(z) \rightarrow zf(z)$. The fact that the first n Landau levels are ideal, when taken together, was first noticed in [25] by explicitly calculating $\text{tr } g = \Omega$ for a $p^2/2m$ particle. This property that adding vortices to the first LL gives components in both first and zeroth LLs is the crux of our generalization.

Definition of First LL Structure— We now precisely define the structure bands must satisfy to be “first Landau level analogues”. A Chern band, with projector P_1 , is *first vortexable* if the following three conditions are satisfied:

1. (Not LLL-like) The band is not vortexable by itself.
2. (\exists Partner Band) There exists an orthogonal vortexable band with projector P_0 (i.e. $P_0 z\Phi_0 = z\Phi_0$ for all $P_0\Phi_0 = \Phi_0$) such that

$$(P_1 + P_0)z\Phi_1 = z\Phi_1 \quad (5)$$

for all states $P_1\Phi_1 = \Phi_1$.

3. (Indecomposability) there is no alternative basis of wavefunctions $(\Phi'_{0\mathbf{k}}, \Phi'_{1\mathbf{k}})$, where each band is vortexable, that also spans the two band subspace of $P_0 + P_1$.

The additional band, described by the projector P_0 , functions as an effective zeroth Landau level, and is emblematic of the fact that first Landau levels always appear with a zeroth Landau level counterpart. Intuitively, acting with z either keeps the wavefunction within the ‘first’ band P_1 or lowers it to the ‘zeroth’ band P_0 — but does not generate components in any other bands (see Fig. 1a). The third condition is in principle necessary to avoid subtle situations where the first two conditions can nominally be realized, but the system should be thought of as a collection of two separate, individually vortexable, bands instead.

While the definition above may appear computationally difficult to verify, an upcoming work will show that wavefunctions that satisfy it are tightly restricted; they are of the form

$$\Phi_1(\mathbf{r}) = Q_0 [(\bar{z}f(z) - 2B_0^{-1}f'(z))\mathcal{N}_0(\mathbf{r}) + f(z)\mathcal{N}_1(\mathbf{r})] \quad (6)$$

where $Q_0 = 1 - P_0$, $\mathcal{N}_{0,1}$ are spinor-valued [cf. Eq. (1)], and P_0 is the projector onto the “zeroth-LL” wavefunctions $f(z)\mathcal{N}_0(\mathbf{r})$. $B_0 = \frac{2\pi}{A_{UC}} = \frac{A_{BZ}}{2\pi}$, and A_{UC} and A_{BZ} are the areas of the unit cell and the Brillouin Zone (BZ), respectively. In Appendix B, we prove that bands with wavefunctions (6) are first vortexable. Bands that are suspected to be first vortexable can be explicitly compared to an instance (6), as we will see shortly.

First vortexability has immediate many-body implications. Consider a first vortexable band that is flat and degenerate with its vortexable counterpart, as in Bernal graphene and in upcoming examples. Let $\Psi_{\nu=2}$ be the many-body state where both bands are full. Now consider the vortex attached state $\Psi_v = \prod_{i < j} (z_i - z_j)^{2s} \Psi_{\nu=p}$ which has filling $p/(2ps+1)$, where $p = 2$ (note, general p follows analogously for $(p-1)$ ’th vortexability). Thanks to vortexability of the combined bands, attaching this vortex factor keeps the final state within the combined bands. The above construction is similar to that of LLL Jain states [63], where projection into the LLL is strictly speaking required at the end. Here however, LLL projection is unnecessary; Ψ_v is an exact zero mode in the limit of short-range interactions [20, 23, 72].

We pause to comment that, while we motivated our definition through the inclusion of Bernal graphene for any value of the interlayer tunneling, as a byproduct we have included bands that for all practical purposes function as zeroth Landau levels (consider the decoupled $\gamma_1 \rightarrow 0$ limit). Interestingly, this limit adiabatically connects Jain-like states with layer-singlet Halperin-like states at $\gamma_1 = 0$. Moreover, γ_1 must be sufficiently large for a Pfaffian outcompete the composite Fermi liquid at half filling [73]. It turns out that the $\gamma_1 \rightarrow \infty$ limit, or more generally $\mathcal{N}_1 \rightarrow 0$, has some additional structure in non-Abelian band geometry that leads to a natural

quantification of how close a band is to the “maximal” first Landau level. In Appendix C, we show that for $\mathcal{N}_1 \rightarrow 0$, the non-Abelian Berry curvature (in the space of the zeroth and first Landau levels) becomes rank deficient, with only one nonzero entry $\hat{\Omega}_{11}$. We can therefore define a “maximality index”

$$M(\mathbf{k}) = \frac{|\lambda_1(\mathbf{k}) - \lambda_2(\mathbf{k})|}{\lambda_1(\mathbf{k}) + \lambda_2(\mathbf{k})}, \quad (7)$$

where $\lambda_{1,2}$ are the eigenvalues of the 2×2 non-Abelian Berry curvature. As γ_1 varies from $0 \rightarrow \infty$ in Bernal graphene, $M(\mathbf{k}) = \gamma_1^2 / (2(v\ell_B^{-1})^2 + \gamma_1^2)$ increases from $0 \rightarrow 1$ (see Appendix D). In general, the maximal $\mathcal{N}_1 \rightarrow 0$ limit corresponds to $M(\mathbf{k}) = 1$.

We expect that first vortexable bands, with $M(\mathbf{k})$ close to 1, will have physics very similar to that of the 1LL. Indeed, for $\mathcal{N}_1 \rightarrow 0$, corresponding to $M(\mathbf{k}) = 1$, the wavefunction (6) effectively differs from the usual first LL only through the modulation $\|\mathcal{N}_0(\mathbf{r})\|/e^{-B_0|\mathbf{r}|^2/4}$, which breaks continuous translation symmetry. LLL states do not seem to be sensitive to such deformations, and so we choose to be optimistic that 1LL states, such as Pfaffian-type topological orders, will be as well.

Analytic Example at Zero Field— To demonstrate first vortexable bands without magnetic fields, we consider an analytically solvable (albeit artificial) example inspired by chiral twisted bilayer graphene. Let

$$H_1 = \begin{pmatrix} 0 & D_1^\dagger \\ D_1 & 0 \end{pmatrix}, \quad D_1 = \begin{pmatrix} D_0 & \gamma_1 I_{2 \times 2} \\ 0 & D_0 \end{pmatrix}. \quad (8)$$

In particular, we assume that D_0 is the chiral Hamiltonian of twisted bilayer graphene (TBG), given by

$$D_0 = \begin{pmatrix} -2i\bar{\partial} & \alpha U_{\omega^*}(\mathbf{r}) \\ \alpha U_{\omega^*}(-\mathbf{r}) & -2i\bar{\partial} \end{pmatrix}, \quad U_{\omega}(\mathbf{r}) = \alpha \sum_{j=0}^2 \omega^j e^{-iq_j \cdot \mathbf{r}} \quad (9)$$

with $\omega = e^{2\pi i/3}$ and $q_{j,x} + iq_{j,y} = -ie^{2\pi j/3}$. While (8) may appear strange due to the upper triangular hoppings connecting non-nearest-“layers”, after a suitable unitary transformation it arises exactly as a $k_z = 0$ band of three dimensional twisted AB-BA double bilayer graphene (see Appendix E). At each magic angle (such as $\alpha \approx 0.586$), D_0 has a zero mode [23, 70, 74]

$$\psi_{0,\mathbf{k}}(r) = \frac{\sigma(z + iB_0^{-1}k)}{\sigma(z)} e^{\frac{i}{2}\bar{k}z} \psi_{\Gamma}(\mathbf{r}), \quad (10)$$

where $k = k_x + ik_y$. The Weierstrass sigma function $\sigma(z)$ satisfies $\sigma(-z) = -\sigma(z)$ and $\sigma(z + R) = \eta_{\mathbf{R}} e^{\frac{\mathbf{R}}{2}(z+R/2)} \sigma(z)$, where $\eta_{\mathbf{R}} = +1$ if $\mathbf{R}/2$ is a lattice vector and -1 otherwise. For each \mathbf{r} , the zero at $k = -iB_0 z$ induces a phase winding of 2π around the BZ, leading to $C = 1$. Moreover, the cell-periodic part $e^{-ik \cdot \mathbf{r}} \psi_{0,\mathbf{k}}(\mathbf{r})$ can be written as a holomorphic functions of k .

Akin to Eq. (3), D_1 has two bands of zero modes. Let $\Phi_{0,\mathbf{k}} = [\psi_{0,\mathbf{k}}, 0]^T$ and $\Phi_{1,\mathbf{k}} = [\gamma_1 \psi_{1,\mathbf{k}}, -\psi_{0,\mathbf{k}}]^T$ where

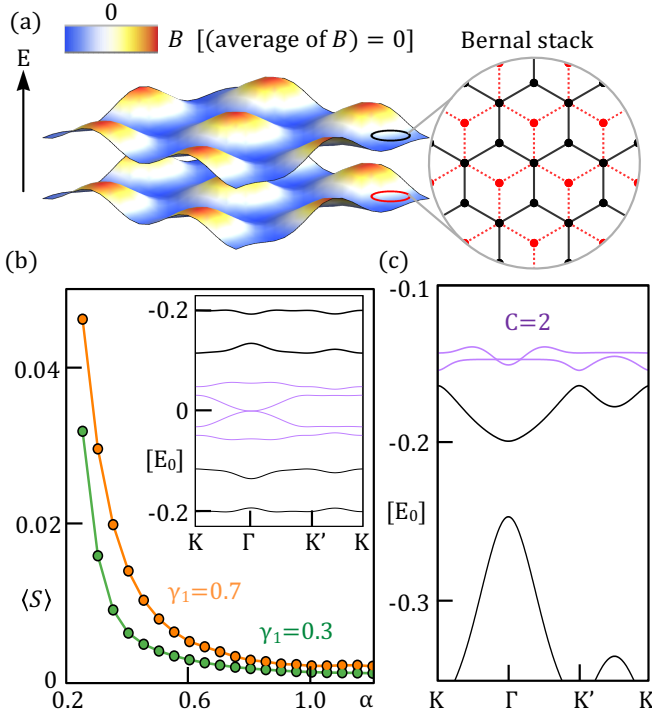


FIG. 2. (a) Bernal graphene with vertical buckling and a strain field, giving a periodic pseudomagnetic field B (color map) with zero average. (b) Average overlap between numerical and analytical approximate zero modes with $\eta = 0.5$, $\langle S \rangle_{\text{BZ}}$, versus α at $\beta = 0$. Inset: bandstructure for $(\alpha, \beta, \gamma) = (0.5, 0, 0.5)$ with low-energy modes $E_{0,1}$ in purple. (c) Bandstructure at $(\alpha, \beta, \gamma) = (0.4, 0.068, 1)$. Displacement field $\beta > 0$ isolates the two low-energy Chern bands (purple).

[75],

$$\psi_{1,\mathbf{k}}(\mathbf{r}) = \left[\bar{z} - \frac{2B_0^{-1}\partial_z\sigma(z + iB_0^{-1}k)}{\sigma(z + iB_0^{-1}k)} - \alpha(\mathbf{k}) \right] \psi_{0,\mathbf{k}}(\mathbf{r}). \quad (11)$$

with $\alpha(\mathbf{k})$ such that $\langle \psi_{0\mathbf{k}} | \psi_{1\mathbf{k}} \rangle = 0$. Then the identity $D_0\psi_{1,\mathbf{k}} = -\psi_{0,\mathbf{k}}$ immediately implies $D_1\Phi_{1,\mathbf{k}} = 0$, giving two bands of zero modes analogous to the LLL and 1LL.

We numerically confirm that Φ_0 and Φ_1 are the zero-modes of H_1 [Eq. (8)] at the magic angle of TBG. There H_1 has four low-energy bands isolated from the remote bands, whose bandwidth vanishes at the same magic angle as TBG, $\alpha = 0.586$ [Fig. 1(b)]. Due to the chiral symmetry of the Hamiltonian, the four eigenstates, denoted by $\Psi_{\pm E_n}$ with the energy $E_n > 0$ ($n = 0, 1$), can be decomposed into sublattice polarized states such as $\Psi_{n\mathbf{k}}^{A,B} = \frac{1}{\sqrt{2}}(\Psi_{E_n,\mathbf{k}} \pm \sigma_z \Psi_{E_n,\mathbf{k}})$. In Fig. 1(b), we plot the bandwidth and the average of $1 - |\langle \Psi_{n\mathbf{k}}^A | \Phi_{n\mathbf{k}} \rangle|$ over the BZ, denoted by $\langle T_n \rangle_{\text{BZ}}$. At the magic angle $\Psi_{n\mathbf{k}}^A = \Phi_{n\mathbf{k}}$ exactly, as expected.

Periodically Strained Bernal Graphene— We will now show how a first vortexable band appears amongst the low energy bands of periodically strained

bilayer graphene [76]. We will take a similar approach to Ref. [77] which studied periodically strained monolayer graphene with a C_2 -breaking substrate that induces C_2 breaking pseudomagnetic field

$$\mathcal{B}(z, \bar{z}) = \mathcal{B}_0 \sum_{l=0}^5 e^{i\mathbf{G}_l \cdot \mathbf{r}} = \mathcal{B}_0 \sum_{l=0}^5 e^{\frac{i}{2}(\mathbf{G}_l \bar{z} + \bar{\mathbf{G}}_l z)} \quad (12)$$

where $\mathbf{G}_l = R_{2\pi l/6} \mathbf{G}_0$, $\mathbf{G}_0 = \frac{4\pi}{\sqrt{3}L_M}(1, 0)$ are smallest reciprocal lattice vectors in terms of the period L_M ; the addition of higher harmonics are not expected to change our conclusions [77]. We note that $\mathcal{B}(\mathbf{r}) = \mathcal{B}(-\mathbf{r})$, within a valley, implies that the pseudomagnetic field is C_2 -odd. Furthermore, $\mathcal{B}(\mathbf{r})$ averages to zero such that the bands we will obtain are Bloch bands, not Landau levels. The periodic strain can be realized by placing monolayer graphene on a lattice of nanorods [78], or by spontaneous buckling of a graphene sheet on C_2 breaking substrates such as NbSe₂ [79]. We will also include a spatially-varying scalar potential proportional to $V(\mathbf{r}) = \sum_l e^{i\mathbf{G}_l \cdot \mathbf{r}}$ and of strength V_0 . The scalar potential could come from patterned gates [80–84], or an electric field that couples to the buckling height.

The (de-dimensionalized) Hamiltonian for AB-stacked graphene's K valley is then

$$H_{\text{SBG}} = E_0 \begin{pmatrix} h - \frac{1}{2}u_0 & \gamma_1\sigma_+ \\ \gamma_1\sigma_- & h + \frac{1}{2}u_0 \end{pmatrix}, \quad (13)$$

$$h = \boldsymbol{\sigma} \cdot [-i\nabla + \alpha\mathcal{A}] - \beta V(\mathbf{r}),$$

where $E_0 = \hbar v_F |\mathbf{G}_0|$, $\sigma_{\pm} = \frac{1}{2}(\sigma_x \pm i\sigma_y)$, $\alpha = 1/\ell_B^2 |G_0|^2$, $\beta = V_0/E_0$, $\mathcal{B}_0 = \hbar/e\ell_B^2$, $\mathcal{A} = \mathcal{A}_x + i\mathcal{A}_y = \sum_l e^{2\pi i l/l} e^{i\mathbf{G}_l \cdot \mathbf{r}}$. We have kept only the dominant on-site interlayer tunneling, with strength $E_0\gamma_1 \approx 370$ meV. The experiment on graphene buckled on NbSe₂ [79] suggests $E_0 \approx 300$ meV and $\alpha \approx 0.4$, which we will use moving forward. We will neglect u_0 for simplicity, consistent with patterned dielectric gates sandwiching the sample. We will set the Γ point of the mini BZ to be the location of the K -valley Dirac point.

A numerical calculation of the $\beta = 0$ band structure (Fig. 3(a)) shows four bands near zero energy and one protected zero mode at the Γ point quadratic band touching. The energy of the four bands decreases exponentially with increasing α , a fact which we will explain shortly, such that for sufficiently large α they should be understood as a near-degenerate four-dimensional low energy subspace that the displacement fields and Coulomb interactions should be projected onto. We will now derive the single particle wavefunctions of this four dimensional subspace.

At $\beta = 0$ the chiral symmetry of the model allows us to write

$$H_{\text{SBG}} = E_0 \begin{pmatrix} 0 & D_1^\dagger \\ D_1 & 0 \end{pmatrix}, \quad D_1 = \begin{pmatrix} D_0 & \gamma_1 \\ 0 & D_0 \end{pmatrix} \quad (14)$$

$$D_0 = -2i\bar{\partial} + \alpha\mathcal{A}.$$

We will obtain the low energy subspace through sublattice polarized near-zero modes of D_1 and D_1^\dagger . We will begin with D_1 . At the Γ point, there is an exact zero mode of D_0 , $\psi_{0,\Gamma}(\mathbf{r}) = e^{-\alpha V(\mathbf{r})}$, and an associated zero mode of D_1 (and thus H) by placing $\psi_{0,\Gamma}$ in the top layer component. We now create two near zero modes, for large α , under the approximation $\psi_{0,\Gamma}(\mathbf{r} = 0) = e^{-6\alpha} \approx 0$; where here and below “ \approx ” specifically means “up to terms of $O(e^{-6\alpha})$ ”. We will use the modified state $\psi_\eta = f_\eta(\mathbf{r})e^{-\alpha V(\mathbf{r})}$, where $f_\eta(\mathbf{r}) = 0$ near $\mathbf{r} = 0$ but is 1 otherwise (e.g. $f_\eta(\mathbf{r}) = \tanh \eta|\mathbf{r}|$ for $\eta \gg 1$). Then, $D_0\psi_\eta \approx 0$, and moreover $D_0\psi_{0,\mathbf{k}}(\mathbf{r}) \approx 0$ where

$$\psi_{0,\mathbf{k}}(\mathbf{r}) = \frac{\sigma(z + iB_0^{-1}k)}{\sigma(z)} e^{\frac{i}{2}\bar{k}z} \psi_\eta(r).$$

Here we used that holomorphic functions commute through D_0 , and $\psi_\eta(0) = 0$. As in the previous section, we can construct

$$\Phi_{0,\mathbf{k}}(\mathbf{r}) = \begin{pmatrix} \psi_{0,\mathbf{k}}(\mathbf{r}) \\ 0 \end{pmatrix}, \quad \Phi_{1,\mathbf{k}}(\mathbf{r}) = \begin{pmatrix} \gamma_1 \psi_{1,\mathbf{k}}(\mathbf{r}) \\ -\psi_{0,\mathbf{k}}(\mathbf{r}) \end{pmatrix}, \quad (15)$$

that satisfy $D_1\Phi_{(0,1),\mathbf{k}}(\mathbf{r}) \approx 0$. In contrast, the B sublattice wavefunctions are topologically trivial; the exact zero mode $\chi_\Gamma = e^{+\alpha V}$ is strongly localized at $\mathbf{r} = 0$ such that $\chi_{0,\mathbf{k}}(\mathbf{r}) = e^{i\mathbf{k}\cdot\mathbf{r}}e^{\alpha V(\mathbf{r})}$ satisfies $D_0^\dagger\chi_{0,\mathbf{k}} = 0$. We can then similarly construct two approximate, topologically trivial, zero modes of D_1^\dagger .

We have therefore constructed two states on the A sublattice that are zero modes up to corrections of order $e^{-6\alpha}$ (and two other states on the B sublattice). The corrections strongly mix the four near-zero modes into energy eigenstates, but do not change the total low-energy subspace significantly. We test this by first extracting sublattice polarized states through $\Psi_n^{A,B} = \frac{1}{\sqrt{2}}(\Psi_{E_n,\mathbf{k}} \pm \sigma_z \Psi_{E_n,\mathbf{k}})$, where $n = 0, 1$ labels the two eigenstates of smallest $E_n > 0$, and $\sigma_z \Psi_{E_n} \propto \Psi_{-E_n}$. Then, focusing on the A sublattice, we calculate $S_{\mathbf{k}}[\Phi_{\mathbf{k}}, \Psi_{\mathbf{k}}^A] = 1 - \text{Tr}[P_{\Phi_{\mathbf{k}}} P_{\Psi_{\mathbf{k}}^A}]/2$ with $P_{\Psi_{\mathbf{k}}^A} = \sum_n |\Psi_{n,\mathbf{k}}^A\rangle\langle\Psi_{n,\mathbf{k}}^A|$ and $P_{\Phi_{\mathbf{k}}} = \sum_n |\Phi_{n,\mathbf{k}}\rangle\langle\Phi_{n,\mathbf{k}}|$. The energy eigenstates are approximate linear combinations of our analytical states if and only if $S_{\mathbf{k}} \approx 0$. In Fig. 3(b), we plot the $\langle S \rangle_{\text{BZ}}$ with $\eta = 0.5$, given by the average of $S_{\mathbf{k}}$ over BZ. $\langle S \rangle_{\text{BZ}} \approx 0.01$ for α as small as 0.2, and it exponentially decreases for larger α .

Since the Dirac cone is protected only by chiral symmetry, tuning $\beta > 0$ energetically shifts Ψ_n^A and Ψ_n^B ($n = 0, 1$) to the hole and electron side, respectively, isolating a complex of two bands that originated from $\Psi_{(0,1)}^A$ with $C = 2$ in total. Fig. 2 shows the bandstructure at $\beta = 0.068$, where bandwidth of the $C = 2$ complex is minimized [77], but the two bands are not separated.

We now show that Coulomb interactions split the two A sublattice bands into bands that are essentially equivalent to Φ_0 and Φ_1 , which are vortexable and first vortexable respectively. This type of splitting is known to occur in Bernal graphene, where the zeroth and first Landau level are degenerate, due to the wavefunctions of the

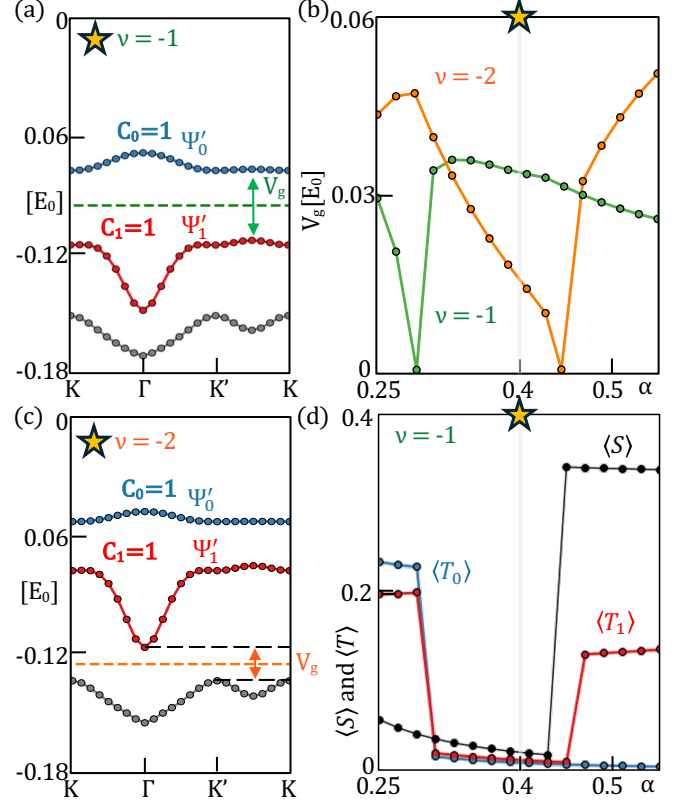


FIG. 3. (a),(c): SCHF bandstructures for $\nu = -1$ and $\nu = -2$, respectively, with parameters corresponding to Fig. 2(c), and $(d, \epsilon_r) = (250 \text{ \AA}, 15)$. The dashed lines represent the Fermi energy. (b) Average overlap between numerical and analytical eigenstate with $\eta = 0.5$, $\langle T_0 \rangle_{\text{BZ}}$ (red) and $\langle T_1 \rangle_{\text{BZ}}$ (blue), at $\nu = -1$ as a function of α . The black line denotes $\langle S \rangle_{\text{BZ}}$. (d) The band gap V_g in (a) and (c) are plotted with green and orange lines.

zeroth LL inducing less exchange energy [85–87]. We consider realistic gate-screened Coulomb interactions:

$$\hat{H}_{\text{tot}} = \hat{H}_{\text{SBG}} + \frac{1}{2A} \sum_{\mathbf{q}} V_{\mathbf{q}} : \hat{\rho}_{\mathbf{q}} \hat{\rho}_{-\mathbf{q}} :, \quad V_{\mathbf{q}} = \frac{2\pi \tanh(qd)}{\epsilon_r \epsilon_0 q} \quad (16)$$

with density operator $\rho_{\mathbf{q}}$ at wavevector \mathbf{q} , normal ordering relative to filling $\nu = 0$, sample area A , gate distance $d = 250 \text{ \AA}$, and relative permittivity $\epsilon_r = 15$. To obtain the two isolated Chern bands, we employ self-consistent Hartree-Fock (SCHF) calculations on 24×24 unit cells. We assume spin and valley polarization [77], and project to well-isolated subspace of the three highest valence bands.

Fig. 3 shows the SCHF bandstructure at filling $\nu = -1$ (a) and $\nu = -2$ (c). As anticipated, interactions split the $C = 2$ complex found at $\nu = 0$ into two isolated bands, both with $C = 1$. Fig. 3(b) shows the SCHF bandgap at $\nu = -2$ closes near $\alpha \approx 0.45$, enabling a topological transition $C = (1, 1) \rightarrow (1, 0)$ by mixing with the third band. Conversely, the top two bands hybridize

to give isolated bands with $C = (2, 0)$ below $\alpha \approx 0.3$. Nevertheless, the two $C = 1$ bands are stable over a range of α for both $\nu = -1$ & -2 .

The two Chern bands form a first vortexable pair to high precision. To check this, we compare the numerical wavefunctions of Fig. 3(a), Ψ'_0 (blue) and Ψ'_1 (red), to the analytic ansätze $\Phi_{(0,1)}$ from Eq. (15). Fig. 3(d) shows the deviation between the numerical and analytic subspaces for both the individual bands $\langle T_{0,1} \rangle_{\text{BZ}}$ and the two-band subspace $\langle S \rangle$, as defined above. In the regime $0.3 < \alpha < 0.45$ with $C = (1, 1)$, the overlap decreases as $O(e^{-5.6\alpha})$, giving deviations $< 1\%$ for $\alpha > 0.38$. As expected, the topological transitions dramatically alter the wavefunction character. The numerical wavefunctions therefore match the analytic ones to extremely good precision, and the latter are vortexable and first vortexable — showing these bands are precisely analogous to the zeroth and first Landau levels. The maximality index for the first vortexable band is $\langle M \rangle_{\text{BZ}} \approx 0.65$ at $\gamma_1 = 1$.

In this work we have proposed “first vortexability” — a precise definition of when a Chern band has the essential character of the first Landau level. First vortexable bands are defined by their quantum geometric data, and each requires a partner band analogous to the zeroth

Landau level. Our examples, both analytic and physically reasonable, suggest such bands are experimentally realizable. Future work will investigate the many-body physics of partially-filled first vortexable bands, particularly at half filling where non-Abelian states are likely.

ACKNOWLEDGMENTS

We thank Jie Wang, Tomohiro Soejima, and Mike Zaletel for enlightening discussions. D.E.P. is supported by the Simons Collaboration on UltraQuantum Matter, which is a grant from the Simons Foundation. D.E.P. is supported by startup funds from the University of California, San Diego. This work was supported by JSPS KAKENHI grant no. JP23KJ0339 and the Center for the Advancement of Topological Semimetals (CATS), an Energy Frontier Research Center at the Ames National Laboratory. Work at the Ames National Laboratory is supported by the U.S. Department of Energy (DOE), Basic Energy Sciences (BES) and is operated for the U.S. DOE by Iowa State University under Contract No. DE-AC02-07CH11358.

-
- [1] B. I. Halperin and J. K. Jain, *Fractional Quantum Hall Effects: New Developments* (World Scientific, 2020).
- [2] S. A. Parameswaran, R. Roy, and S. L. Sondhi, Fractional quantum hall physics in topological flat bands, *Comptes Rendus Physique* **14**, 816 (2013).
- [3] E. J. Bergholtz and Z. Liu, Topological flat band models and fractional chern insulators, *International Journal of Modern Physics B* **27**, 1330017 (2013).
- [4] T. Neupert, C. Chamon, T. Iadecola, L. H. Santos, and C. Mudry, Fractional (chern and topological) insulators, *Physica Scripta* **T164**, 014005 (2015).
- [5] Z. Liu and E. J. Bergholtz, Recent developments in fractional chern insulators, in *Reference Module in Materials Science and Materials Engineering* (Elsevier, 2023).
- [6] T. Neupert, L. Santos, C. Chamon, and C. Mudry, Fractional quantum hall states at zero magnetic field, *Phys. Rev. Lett.* **106**, 236804 (2011).
- [7] D. Sheng, Z.-C. Gu, K. Sun, and L. Sheng, Fractional quantum hall effect in the absence of landau levels, *Nature communications* **2**, 389 (2011).
- [8] N. Regnault and B. A. Bernevig, Fractional chern insulator, *Physical Review X* **1**, 021014 (2011).
- [9] E. Tang, J.-W. Mei, and X.-G. Wen, High-temperature fractional quantum hall states, *Physical review letters* **106**, 236802 (2011).
- [10] K. Sun, Z. Gu, H. Katsura, and S. D. Sarma, Nearly flat-bands with nontrivial topology, *Physical review letters* **106**, 236803 (2011).
- [11] E. M. Spanton, A. A. Zibrov, H. Zhou, T. Taniguchi, K. Watanabe, M. P. Zaletel, and A. F. Young, Observation of fractional chern insulators in a van der waals heterostructure, *Science* **360**, 62 (2018).
- [12] Y. Xie, A. T. Pierce, J. M. Park, D. E. Parker, E. Khalaf, P. Ledwith, Y. Cao, S. H. Lee, S. Chen, P. R. Forrester, *et al.*, Fractional chern insulators in magic-angle twisted bilayer graphene, *Nature* **600**, 439 (2021).
- [13] J. Cai, E. Anderson, C. Wang, X. Zhang, X. Liu, W. Holtzmann, Y. Zhang, F. Fan, T. Taniguchi, K. Watanabe, *et al.*, Signatures of fractional quantum anomalous hall states in twisted MoTe₂, *Nature* **622**, 63 (2023).
- [14] Y. Zeng, Z. Xia, K. Kang, J. Zhu, P. Knüppel, C. Vaswani, K. Watanabe, T. Taniguchi, K. F. Mak, and J. Shan, Thermodynamic evidence of fractional chern insulator in moiré MoTe₂, *Nature* **622**, 69 (2023).
- [15] H. Park, J. Cai, E. Anderson, Y. Zhang, J. Zhu, X. Liu, C. Wang, W. Holtzmann, C. Hu, Z. Liu, *et al.*, Observation of fractionally quantized anomalous hall effect, *Nature* **622**, 74 (2023).
- [16] F. Xu, Z. Sun, T. Jia, C. Liu, C. Xu, C. Li, Y. Gu, K. Watanabe, T. Taniguchi, B. Tong, *et al.*, Observation of integer and fractional quantum anomalous hall effects in twisted bilayer MoTe₂, *Physical Review X* **13**, 031037 (2023).
- [17] Z. Lu, T. Han, Y. Yao, A. P. Reddy, J. Yang, J. Seo, K. Watanabe, T. Taniguchi, L. Fu, and L. Ju, Fractional quantum anomalous hall effect in a graphene moire superlattice, arXiv preprint arXiv:2309.17436 [10.48550/arXiv.2309.17436](https://arxiv.org/abs/2309.17436) (2023).
- [18] D. Parker, P. Ledwith, E. Khalaf, T. Soejima, J. Hauschild, Y. Xie, A. Pierce, M. P. Zaletel, A. Yacoby, and A. Vishwanath, Field-tuned and zero-field fractional chern insulators in magic angle graphene, arXiv preprint arXiv:2112.13837 [10.48550/arXiv.2112.13837](https://arxiv.org/abs/2112.13837) (2021).
- [19] J. Wang, J. Cano, A. J. Millis, Z. Liu, and B. Yang, Exact landau level description of geometry and interaction in a

- flatband, *Physical review letters* **127**, 246403 (2021).
- [20] P. J. Ledwith, A. Vishwanath, and D. E. Parker, Vortexability: A unifying criterion for ideal fractional chern insulators, *Physical Review B* **108**, 205144 (2023).
- [21] R. Roy, Band geometry of fractional topological insulators, *Physical Review B* **90**, 165139 (2014).
- [22] M. Claassen, C. H. Lee, R. Thomale, X.-L. Qi, and T. P. Devereaux, Position-momentum duality and fractional quantum hall effect in chern insulators, *Physical review letters* **114**, 236802 (2015).
- [23] P. J. Ledwith, G. Tarnopolsky, E. Khalaf, and A. Vishwanath, Fractional chern insulator states in twisted bilayer graphene: An analytical approach, *Physical Review Research* **2**, 023237 (2020).
- [24] P. J. Ledwith, E. Khalaf, and A. Vishwanath, Strong coupling theory of magic-angle graphene: A pedagogical introduction, *Annals of Physics* **435**, 168646 (2021).
- [25] T. Ozawa and B. Mera, Relations between topology and the quantum metric for chern insulators, *Physical Review B* **104**, 045103 (2021).
- [26] B. Mera and T. Ozawa, Kähler geometry and chern insulators: Relations between topology and the quantum metric, *Physical Review B* **104**, 045104 (2021).
- [27] B. Mera and T. Ozawa, Engineering geometrically flat chern bands with fubini-study kähler structure, *Physical Review B* **104**, 115160 (2021).
- [28] P. J. Ledwith, A. Vishwanath, and E. Khalaf, Family of ideal chern flatbands with arbitrary chern number in chiral twisted graphene multilayers, *Physical Review Letters* **128**, 176404 (2022).
- [29] B. Mera and T. Ozawa, Uniqueness of landau levels and their analogs with higher chern numbers, arXiv preprint arXiv:2304.00866 [10.48550/arXiv.2304.00866](https://arxiv.org/abs/10.48550/arXiv.2304.00866) (2023).
- [30] H. Li, U. Kumar, K. Sun, and S.-Z. Lin, Spontaneous fractional chern insulators in transition metal dichalcogenide moiré superlattices, *Physical Review Research* **3**, L032070 (2021).
- [31] V. Crépel and L. Fu, Anomalous hall metal and fractional chern insulator in twisted transition metal dichalcogenides, *Physical Review B* **107**, L201109 (2023).
- [32] J. Dong, J. Wang, P. J. Ledwith, A. Vishwanath, and D. E. Parker, Composite fermi liquid at zero magnetic field in twisted MoTe₂, *Phys. Rev. Lett.* **131**, 136502 (2023).
- [33] H. Goldman, A. P. Reddy, N. Paul, and L. Fu, Zero-field composite fermi liquid in twisted semiconductor bilayers, *Phys. Rev. Lett.* **131**, 136501 (2023).
- [34] X. Hu, D. Xiao, and Y. Ran, Hyperdeterminants and composite fermion states in fractional chern insulators, arXiv preprint arXiv:2312.00636 [10.48550/arXiv.2312.00636](https://arxiv.org/abs/10.48550/arXiv.2312.00636) (2023).
- [35] X.-Y. Song, C.-M. Jian, L. Fu, and C. Xu, Intertwined fractional quantum anomalous hall states and charge density waves, arXiv preprint arXiv:2310.11632 [10.48550/arXiv.2310.11632](https://arxiv.org/abs/10.48550/arXiv.2310.11632) (2023).
- [36] N. Mao, C. Xu, J. Li, T. Bao, P. Liu, Y. Xu, C. Felser, L. Fu, and Y. Zhang, Lattice relaxation, electronic structure and continuum model for twisted bilayer MoTe₂, arXiv preprint arXiv:2311.07533 [10.48550/arXiv.2311.07533](https://arxiv.org/abs/10.48550/arXiv.2311.07533) (2023).
- [37] J. Yu, J. Herzog-Arbeitman, M. Wang, O. Vafek, B. A. Bernevig, and N. Regnault, Fractional chern insulators vs. non-magnetic states in twisted bilayer MoTe₂, arXiv preprint arXiv:2309.14429 [10.48550/arXiv.2309.14429](https://arxiv.org/abs/10.48550/arXiv.2309.14429) (2023).
- [38] N. Morales-Durán, N. Wei, and A. H. MacDonald, Magic angles and fractional chern insulators in twisted homobilayer tmds, arXiv preprint arXiv:2308.03143 [10.48550/arXiv.2308.03143](https://arxiv.org/abs/10.48550/arXiv.2308.03143) (2023).
- [39] Y. Jia, J. Yu, J. Liu, J. Herzog-Arbeitman, Z. Qi, N. Regnault, H. Weng, B. A. Bernevig, and Q. Wu, Moiré fractional chern insulators I: First-principles calculations and continuum models of twisted bilayer MoTe₂, arXiv preprint arXiv:2311.04958 [10.48550/arXiv.2311.04958](https://arxiv.org/abs/10.48550/arXiv.2311.04958) (2023).
- [40] C. Xu, J. Li, Y. Xu, Z. Bi, and Y. Zhang, Maximally localized wannier functions, interaction models, and fractional quantum anomalous hall effect in twisted bilayer MoTe₂, *Proceedings of the National Academy of Sciences* **121**, e2316749121 (2024).
- [41] C. Wang, X.-W. Zhang, X. Liu, Y. He, X. Xu, Y. Ran, T. Cao, and D. Xiao, Fractional chern insulator in twisted bilayer MoTe₂, *Physical Review Letters* **132**, 036501 (2024).
- [42] H. Li, Y. Su, Y. B. Kim, H.-Y. Kee, K. Sun, and S.-Z. Lin, Contrasting twisted bilayer graphene and transition metal dichalcogenides for fractional chern insulators: an emergent gauge picture, arXiv preprint arXiv:2402.02251 [10.48550/arXiv.2402.02251](https://arxiv.org/abs/10.48550/arXiv.2402.02251) (2024).
- [43] Z. Dong, A. S. Patri, and T. Senthil, Theory of fractional quantum anomalous hall phases in pentalayer rhombohedral graphene moiré structures, arXiv preprint arXiv:2311.03445 [10.48550/arXiv.2311.03445](https://arxiv.org/abs/10.48550/arXiv.2311.03445) (2023).
- [44] B. Zhou, H. Yang, and Y.-H. Zhang, Fractional quantum anomalous hall effects in rhombohedral multilayer graphene in the moiréless limit and in coulomb imprinted superlattice, arXiv preprint arXiv:2311.04217 [10.48550/arXiv.2311.04217](https://arxiv.org/abs/10.48550/arXiv.2311.04217) (2023).
- [45] J. Dong, T. Wang, T. Wang, T. Soejima, M. P. Zaletel, A. Vishwanath, and D. E. Parker, Anomalous hall crystals in rhombohedral multilayer graphene I: Interaction-driven chern bands and fractional quantum hall states at zero magnetic field, arXiv preprint arXiv:2311.05568 [10.48550/arXiv.2311.05568](https://arxiv.org/abs/10.48550/arXiv.2311.05568) (2023).
- [46] J. Herzog-Arbeitman, Y. Wang, J. Liu, P. M. Tam, Z. Qi, Y. Jia, D. K. Efetov, O. Vafek, N. Regnault, H. Weng, *et al.*, Moiré fractional chern insulators II: First-principles calculations and continuum models of rhombohedral graphene superlattices, arXiv preprint arXiv:2311.12920 [10.48550/arXiv.2311.12920](https://arxiv.org/abs/10.48550/arXiv.2311.12920) (2023).
- [47] Y. H. Kwan, J. Yu, J. Herzog-Arbeitman, D. K. Efetov, N. Regnault, and B. A. Bernevig, Moiré fractional chern insulators III: Hartree-fock phase diagram, magic angle regime for chern insulator states, the role of the Moiré potential and goldstone gaps in rhombohedral graphene superlattices, arXiv preprint arXiv:2312.11617 [10.48550/arXiv.2312.11617](https://arxiv.org/abs/10.48550/arXiv.2312.11617) (2023).
- [48] Z. Guo, X. Lu, B. Xie, and J. Liu, Theory of fractional chern insulator states in pentalayer graphene moiré superlattice, arXiv preprint arXiv:2311.14368 [10.48550/arXiv.2311.14368](https://arxiv.org/abs/10.48550/arXiv.2311.14368) (2023).
- [49] R. Willett, J. P. Eisenstein, H. L. Störmer, D. C. Tsui, A. C. Gossard, and J. English, Observation of an even-denominator quantum number in the fractional quantum hall effect, *Physical review letters* **59**, 1776 (1987).
- [50] W. Pan, N. Masuhara, N. Sullivan, K. Baldwin, K. West, L. Pfeiffer, and D. Tsui, Impact of disorder on the 5/2 fractional quantum hall state, *Physical review letters*

- 106**, 206806 (2011).
- [51] J. Eisenstein, K. Cooper, L. Pfeiffer, and K. West, Insulating and fractional quantum hall states in the first excited landau level, *Physical Review Letters* **88**, 076801 (2002).
- [52] D.-K. Ki, V. I. Fal'ko, D. A. Abanin, and A. F. Morpurgo, Observation of even denominator fractional quantum hall effect in suspended bilayer graphene, *Nano letters* **14**, 2135 (2014).
- [53] Y. Kim, A. C. Balram, T. Taniguchi, K. Watanabe, J. K. Jain, and J. H. Smet, Even denominator fractional quantum hall states in higher landau levels of graphene, *Nature Physics* **15**, 154 (2019).
- [54] A. A. Zibrov, C. Kometter, H. Zhou, E. Spanton, T. Taniguchi, K. Watanabe, M. Zaletel, and A. Young, Tunable interacting composite fermion phases in a half-filled bilayer-graphene landau level, *Nature* **549**, 360 (2017).
- [55] J. Li, C. Tan, S. Chen, Y. Zeng, T. Taniguchi, K. Watanabe, J. Hone, and C. Dean, Even-denominator fractional quantum hall states in bilayer graphene, *Science* **358**, 648 (2017).
- [56] K. Huang, H. Fu, D. R. Hickey, N. Alem, X. Lin, K. Watanabe, T. Taniguchi, and J. Zhu, Valley isospin controlled fractional quantum hall states in bilayer graphene, *Physical Review X* **12**, 031019 (2022).
- [57] G. Moore and N. Read, Nonabelions in the fractional quantum hall effect, *Nuclear Physics B* **360**, 362 (1991).
- [58] A. Kumar, G. Csáthy, M. Manfra, L. Pfeiffer, and K. West, Nonconventional odd-denominator fractional quantum hall states in the second landau level, *Physical review letters* **105**, 246808 (2010).
- [59] N. Read and E. Rezayi, Beyond paired quantum hall states: Parafermions and incompressible states in the first excited landau level, *Physical Review B* **59**, 8084 (1999).
- [60] R. S. Mong, M. P. Zaletel, F. Pollmann, and Z. Papić, Fibonacci anyons and charge density order in the 12/5 and 13/5 quantum hall plateaus, *Physical Review B* **95**, 115136 (2017).
- [61] C. Nayak, S. H. Simon, A. Stern, M. Freedman, and S. D. Sarma, Non-abelian anyons and topological quantum computation, *Reviews of Modern Physics* **80**, 1083 (2008).
- [62] R. S. Mong, D. J. Clarke, J. Alicea, N. H. Lindner, P. Fendley, C. Nayak, Y. Oreg, A. Stern, E. Berg, K. Shtengel, *et al.*, Universal topological quantum computation from a superconductor-abelian quantum hall heterostructure, *Physical Review X* **4**, 011036 (2014).
- [63] J. K. Jain, Composite-fermion approach for the fractional quantum hall effect, *Phys. Rev. Lett.* **63**, 199 (1989).
- [64] D. Varjas, A. Abouelkomsan, K. Yang, and E. J. Bergholtz, Topological lattice models with constant Berry curvature, *SciPost Phys.* **12**, 118 (2022).
- [65] Y. Sheffer, R. Queiroz, and A. Stern, Symmetries as the guiding principle for flattening bands of dirac fermions, *Physical Review X* **13**, 021012 (2023).
- [66] B. Estienne, N. Regnault, and V. Crépel, Ideal chern bands as landau levels in curved space, *Phys. Rev. Res.* **5**, L032048 (2023).
- [67] H. Liu, K. Yang, A. Abouelkomsan, Z. Liu, and E. J. Bergholtz, Broken symmetry in ideal chern bands, arXiv preprint arXiv:2402.04303 [10.48550/arXiv.2402.04303](https://arxiv.org/abs/10.48550/arXiv.2402.04303) (2024).
- [68] S. A. Parameswaran, R. Roy, and S. L. Sondhi, Fractional quantum hall physics in topological flat bands, *Comptes Rendus. Physique* **14**, 816–839 (2013).
- [69] R. Roy, Band geometry of fractional topological insulators, *Phys. Rev. B* **90**, 165139 (2014).
- [70] G. Tarnopolsky, A. J. Kruchkov, and A. Vishwanath, Origin of magic angles in twisted bilayer graphene, *Phys. Rev. Lett.* **122**, 106405 (2019).
- [71] S. H. Simon and M. S. Rudner, Contrasting lattice geometry dependent versus independent quantities: Ramifications for berry curvature, energy gaps, and dynamics, *Phys. Rev. B* **102**, 165148 (2020).
- [72] S. A. Trugman and S. Kivelson, Exact results for the fractional quantum hall effect with general interactions, *Phys. Rev. B* **31**, 5280 (1985).
- [73] Z. Zhu, D. N. Sheng, and I. Sodemann, Widely tunable quantum phase transition from moore-read to composite fermi liquid in bilayer graphene, *Phys. Rev. Lett.* **124**, 097604 (2020).
- [74] J. Wang, Y. Zheng, A. J. Millis, and J. Cano, Chiral approximation to twisted bilayer graphene: Exact intravalley inversion symmetry, nodal structure, and implications for higher magic angles, *Phys. Rev. Res.* **3**, 023155 (2021).
- [75] We note $\psi_{1,\mathbf{k}}$ obeys the Bloch condition because the shift in $z \rightarrow z + R$ in the first term is cancelled out by
- $$\partial_z \sigma(z + R) = -e^{\frac{B_0}{2} \bar{R}(z+R/2)} \left[\partial_z \sigma(z) - \frac{B_0}{2} \bar{R} \sigma(z) \right]. \quad (17)$$
- [76] X. Wan, S. Sarkar, K. Sun, and S.-Z. Lin, Nearly flat chern band in periodically strained monolayer and bilayer graphene, *Phys. Rev. B* **108**, 125129 (2023).
- [77] Q. Gao, J. Dong, P. Ledwith, D. Parker, and E. Khalaf, Untwisting moiré physics: Almost ideal bands and fractional chern insulators in periodically strained monolayer graphene, *Physical Review Letters* **131**, 096401 (2023).
- [78] Y. Jiang, J. Mao, J. Duan, X. Lai, K. Watanabe, T. Taniguchi, and E. Y. Andrei, Visualizing strain-induced pseudomagnetic fields in graphene through an hbn magnifying glass, *Nano letters* **17**, 2839 (2017).
- [79] J. Mao, S. P. Milovanović, M. Anđelković, X. Lai, Y. Cao, K. Watanabe, T. Taniguchi, L. Covaci, F. M. Peeters, A. K. Geim, Y. Jiang, and E. Y. Andrei, Evidence of flat bands and correlated states in buckled graphene superlattices, *Nature* **584**, 215 (2020).
- [80] C. Forsythe, X. Zhou, K. Watanabe, T. Taniguchi, A. Papsupathy, P. Moon, M. Koshino, P. Kim, and C. R. Dean, Band structure engineering of 2d materials using patterned dielectric superlattices, *Nature nanotechnology* **13**, 566 (2018).
- [81] L.-k. Shi, J. Ma, and J. C. Song, Gate-tunable flat bands in van der waals patterned dielectric superlattices, *2D Materials* **7**, 015028 (2019).
- [82] J. Cano, S. Fang, J. Pixley, and J. H. Wilson, Moiré superlattice on the surface of a topological insulator, *Physical Review B* **103**, 155157 (2021).
- [83] D. Guerci, J. Wang, J. Pixley, and J. Cano, Designer meron lattice on the surface of a topological insulator, *Physical Review B* **106**, 245417 (2022).
- [84] S. A. A. Ghorashi and J. Cano, Multilayer graphene with a superlattice potential, *Physical Review B* **107**, 195423 (2023).
- [85] Y. Barlas, R. Côté, K. Nomura, and A. H. MacDonald,

ald, Intra-landau-level cyclotron resonance in bilayer graphene, *Phys. Rev. Lett.* **101**, 097601 (2008).

- [86] Y. Barlas, K. Yang, and A. H. MacDonald, Quantum hall effects in graphene-based two-dimensional electron systems, *Nanotechnology* **23**, 052001 (2012).
- [87] B. M. Kousa, N. Wei, and A. H. MacDonald, Orbital competition in bilayer graphene's fractional quantum hall effect, arXiv preprint arXiv:2402.10440 [10.48550/arXiv.2402.10440](https://arxiv.org/abs/2402.10440) (2024).
- [88] J. Dong, P. J. Ledwith, E. Khalaf, J. Y. Lee, and A. Vishwanath, Many-body ground states from decomposition of ideal higher chern bands: Applications to chirally twisted graphene multilayers, *Phys. Rev. Res.* **5**, 023166 (2023).
- [89] M. Koshino, Band structure and topological properties of twisted double bilayer graphene, *Physical Review B* **99**, 235406 (2019).

Appendix A: Multi-band Vortexable Band Geometry

In this section we review ideal, or vortexable, band geometry for multiple bands and study the non-Abelian quantum geometric tensor in this context for later use. The non-Abelian quantum geometric tensor (QGT) is given, in an orthonormal basis, as

$$\begin{aligned}\hat{\eta}_{ab}^{\mu\nu} &= \langle \partial_{k_\nu} u_{kb} | Q(\mathbf{k}) | \partial_{k_\mu} u_{ka} \rangle, \\ Q(\mathbf{k}) &= 1 - \sum_a |u_{ka}\rangle \langle u_{ka}| \end{aligned} \quad (\text{A1})$$

where a, b are band-indices.

We will denote its trace by removing its hat, or with a capital Tr, i.e.

$$\eta^{\mu\nu} = \text{Tr } \hat{\eta}^{\mu\nu} = \sum_a \eta_{aa}^{\mu\nu}. \quad (\text{A2})$$

Note that our gauge-covariance based definition of $\hat{\eta}$ ensures that $\eta^{\mu\nu}$ is gauge invariant, even in non-orthonormal bases. The non-Abelian Berry curvature and metric are defined with the symmetric and antisymmetric components in the spatial indices

$$\begin{aligned}\hat{g}^{\mu\nu}(\mathbf{k}) &= \frac{1}{2}(\hat{\eta}^{\mu\nu} + \hat{\eta}^{\nu\mu}) \\ \hat{\Omega}_{ab}\varepsilon^{\mu\nu} &= i(\hat{\eta}^{\mu\nu} - \hat{\eta}^{\nu\mu}) \end{aligned} \quad (\text{A3})$$

We now claim the following conditions are equivalent [19, 20, 25, 26, 28]

- (V1) The bands are vortexable: $z\psi = Pz\psi$, where $\psi = P\psi$ is any wavefunction in the band and P is the band projector.
- (V2) The inequality $\text{tr } g \geq \Omega$, or $\text{tr } \text{Tr } \hat{g} \geq \text{Tr } \hat{\Omega}$, is saturated, where $z + x + iy$ is the vortex function.
- (V3) There is a gauge, in which the wavefunctions are generically non-orthonormal, such that $|u_{ka}\rangle = |u_{ka}\rangle$ are holomorphic functions of $k = k_x + ik_y$.

- (V4) The quantum metric factorizes as $\hat{\eta}_{ab}^{\mu\nu} = \frac{1}{2}\hat{\Omega}_{ab}(\delta_{\mu\nu} - i\varepsilon_{\mu\nu})$, where $\hat{\Omega}_{ab} = \langle \partial_k u_{kb} | Q(\mathbf{k}) | \partial_k u_{ka} \rangle$ is the non-Abelian Berry curvature and $2\partial_k = \partial_{k_x} + i\partial_{k_y}$ is the derivative with respect to $k = k_x + ik_y$

Ref. [20] showed the equivalence between (V1) and (V2), and reviewed the equivalence between (V2) and (V3) through an explicit construction of the required gauge transformation, which was previously shown to exist by Ref. [26]. It remains to show (V4) is equivalent to (V1-3). The implication (V4) \implies (V2) follows immediately by computing $\text{tr } g$ and Ω from the traced symmetric and antisymmetric parts of $\hat{\eta}_{ab}^{\mu\nu} = \frac{1}{2}\hat{\Omega}_{ab}(\delta_{\mu\nu} - i\varepsilon_{\mu\nu})$ respectively. We conclude by showing (V3) \implies (V4); to see this, we use (V3) to write $|u_{\mathbf{k}}\rangle = S_{\mathbf{k}}|\tilde{u}_{\mathbf{k}}\rangle$, where $S_{\mathbf{k}}$ is a matrix that is not necessarily unitary and $|\tilde{u}_{\mathbf{k}}\rangle$ is holomorphic. Then we have

$$\begin{aligned}Q(\mathbf{k})\partial_{k_x}|u_{ka}\rangle &= Q(\mathbf{k})(\partial_k + \bar{\partial}_k)S_{\mathbf{k}}|\tilde{u}_k\rangle \\ &= S_{\mathbf{k}}Q(\mathbf{k})\partial_k|\tilde{u}_{ka}\rangle \\ &= Q(\mathbf{k})\partial_k|u_{ka}\rangle \end{aligned} \quad (\text{A4})$$

where we used that the term coming from differentiating $S(\mathbf{k})$ is annihilated by $Q(\mathbf{k})$. Similarly we can write $Q(\mathbf{k})\partial_{k_y}|u_{\mathbf{k}}\rangle = iQ(\mathbf{k})\partial_k|u_{\mathbf{k}}\rangle$. Substituting into (A2) then yields (V4).

Appendix B: First vortexability of trial wavefunctions

In this section we show explicitly that the trial wavefunctions that we have used throughout the main text are first vortexable. For readability, we recall the definition now. A band is first vortexable if

- (P1) The band is not vortexable by itself
- (P2) There exists an orthogonal vortexable band with projector P_0 (i.e. $P_0z\psi_0 = z\psi_0$ for all $P_0\psi_0 = \psi_0$) such that
- $$(P_1 + P_0)z\psi_1 = z\psi_1 \quad (\text{B1})$$
- for all states $P\psi_1 = \psi_1$
- (P3) There is no alternative basis of wavefunctions $(\phi_{0\mathbf{k}}, \phi_{1\mathbf{k}})$, where each band is vortexable, that also spans the two band subspace $P_0 + P_1$

We begin with a useful Lemma used repeatedly below.

Lemma 1. *A function of crystal momentum that satisfies $f(\mathbf{k} + \mathbf{G}) = f(\mathbf{k}) - i\lambda\bar{G}$ under translation by reciprocal lattice vectors, for some $\lambda \neq 0$, is not holomorphic in $k_x + ik_y$.*

Proof. Consider a contour integral of f around the parallelogram boundary of the BZ, with side lengths G_1 and G_2 , that vanishes for holomorphic functions by Cauchy's

theorem. On the other hand, the shift-periodicity of f relates the integrals on opposite sides of the parallelogram such that

$$\oint_{\partial\text{BZ}} f(\mathbf{k}) d\mathbf{k} = -i\lambda(\overline{G_1}G_2 - \overline{G_2}G_1) = \lambda A_{\text{BZ}} \neq 0. \quad (\text{B2})$$

We conclude that f is not holomorphic \square

We begin by outlining how we will show that the trial wavefunctions $(\Phi_{0\mathbf{k}}, \Phi_{1\mathbf{k}})$ used in the main text are vortexable and first vortexable, respectively. The first step is to show that the various $\Phi_{1\mathbf{k}}(\mathbf{r})$ we have constructed are not vortexable themselves, property (P2) but are when combined with $\Phi_{0\mathbf{k}}(\mathbf{r})$, (P1). It is possible to show this in real space, by acting with z on $\Phi_{1\mathbf{k}}(\mathbf{r})$ and expressing the result as a sum of $\Phi_{1\mathbf{k}}(\mathbf{r})$ and $\Phi_{0\mathbf{k}}(\mathbf{r})$. However, (P3) demands that is no "decomposed" basis, in which the space spanned by $\Phi_{(0,1)\mathbf{k}}(\mathbf{r})$ is split into two bands that are vortexable on their own. To show that such a basis doesn't exist, it is convenient to work in a holomorphic gauge in momentum space as there are powerful no-go results on holomorphic functions. Thus, throughout this section we will use the equivalence of vortexability with the existence of a holomorphic gauge (V3). We note that the wavefunctions in the holomorphic gauge are generically neither normalized nor orthogonal, and gauge transformations are invertible but generically non-unitary.

We note that all trial wavefunctions that we have used have periodic wavefunctions $u_{\mathbf{k}}(\mathbf{r}) = e^{-i\mathbf{k}\cdot\mathbf{r}}\Phi_{\mathbf{k}}(\mathbf{r})$ of the form

$$\begin{aligned} u_{0,\mathbf{k}}(\mathbf{r}) &= f_{\mathbf{k}}(z)\mathcal{N}_0(\mathbf{r}) \\ u_{1,\mathbf{k}}(\mathbf{r}) &= [(\bar{z} - 2B_0^{-1}\partial_z - \alpha(\mathbf{k}))f_{\mathbf{k}}(\mathbf{r})]\mathcal{N}_0(\mathbf{r}) \\ &\quad + f_{\mathbf{k}}(\mathbf{r})\mathcal{N}_1(\mathbf{r}) \end{aligned} \quad (\text{B3})$$

where

$$f_{\mathbf{k}}(\mathbf{r}) = e^{-\frac{i}{2}k\bar{z}}\sigma(z + iB_0^{-1}k). \quad (\text{B4})$$

The function $\alpha(\mathbf{k})$ was chosen so that the states are orthogonal, and the functions $\mathcal{N}_{0,1}^l(\mathbf{r})$ are functions of the layer and real-space but not \mathbf{k} . We note that we can write $(\bar{z} - 2B_0^{-1}\partial_z)f_{\mathbf{k}}(\mathbf{r}) = 2i\partial_k f_{\mathbf{k}}(\mathbf{r})$. This implies that we can form the k -holomorphic states

$$v_{0,\mathbf{k}} = u_{0,\mathbf{k}}, \quad v_{1,\mathbf{k}}(\mathbf{r}) = 2i\partial_k u_{0,\mathbf{k}}(\mathbf{r}) + f_{\mathbf{k}}(\mathbf{r})\mathcal{N}_1(\mathbf{r}) \quad (\text{B5})$$

as an alternative holomorphic basis through dropping $\alpha(\mathbf{k})$.

It is important to emphasize that the wavefunctions $v_{1,\mathbf{k}}^l(\mathbf{r})$ do not describe a vortexable band despite the fact that they are holomorphic in k . Indeed, they do not define a single Bloch band because $v_{1,\mathbf{k}+G}$ is not proportional to $v_{1,\mathbf{k}}$. Using $\sigma(z + R) = \eta_{\mathbf{R}}e^{\frac{\beta}{2}R(z+R/2)}\sigma(z)$, we have that

$$v_{0,\mathbf{k}+G}(\mathbf{r}) = e^{-i\mathbf{G}\cdot\mathbf{r}}\xi_{\mathbf{G}}(k)v_{0,\mathbf{k}}(\mathbf{r})$$

for $\xi_{\mathbf{G}}(k) = \eta_{\mathbf{G}}e^{\frac{1}{2}B^{-1}\overline{G}(k+\frac{G}{2})}$. In contrast,

$$\begin{aligned} v_{1,\mathbf{k}+G}(\mathbf{r}) &= e^{-i\mathbf{G}\cdot\mathbf{r}}(2i\partial_k(\xi_{\mathbf{G}}(k)v_{0,\mathbf{k}} + \xi_{\mathbf{G}}(k)f_{\mathbf{k}}(\mathbf{r})\mathcal{N}_1) \\ &= e^{-i\mathbf{G}\cdot\mathbf{r}}\xi_{\mathbf{G}}(k)(v_{1,\mathbf{k}} + iB_0^{-1}\overline{G}v_{0,\mathbf{k}}) \end{aligned} \quad (\text{B6})$$

where we used $2i\xi_{\mathbf{G}}^{-1}\partial_k\xi_{\mathbf{G}} = iB_0^{-1}\overline{G}$.

The existence of the above holomorphic gauge shows that the entire two band subspace is vortexable, (P2). However, the nonperiodicity allows us to show that $u_{1,\mathbf{k}} = v_{1,\mathbf{k}}(\mathbf{r}) - \alpha(\mathbf{k})v_{0,\mathbf{k}}(\mathbf{r})$ is not vortexable on its own. Indeed, $v_{1,\mathbf{k}}$ is vortexable if and only if $\alpha(\mathbf{k})$ is holomorphic. However, using boundary conditions for $v_{n\mathbf{k}}$, we find $\alpha(\mathbf{k}) = \|v_{0,\mathbf{k}}\|^{-2}\langle v_{0,\mathbf{k}}|v_{1,\mathbf{k}}\rangle$ satisfies $\alpha(\mathbf{k} + \mathbf{G}) = \alpha(\mathbf{k}) + iB_0^{-1}\overline{G}$. Thus Lemma 1 implies α is not holomorphic, and (P1) is satisfied.

We must now prove (P3). This amounts to showing that

$$\begin{pmatrix} w_{0,\mathbf{k}} \\ w_{1,\mathbf{k}} \end{pmatrix} = S_k^{-1} \begin{pmatrix} v_{0,\mathbf{k}} \\ v_{1,\mathbf{k}} \end{pmatrix} \quad (\text{B7})$$

cannot have diagonal boundary conditions,

$$\begin{pmatrix} w_{0,\mathbf{k}+G} \\ w_{1,\mathbf{k}+G} \end{pmatrix} = e^{-i\mathbf{G}\cdot\mathbf{r}} \begin{pmatrix} \tilde{\xi}_{\mathbf{G}}^{(0)}(k) & 0 \\ 0 & \tilde{\xi}_{\mathbf{G}}^{(1)}(k) \end{pmatrix} \begin{pmatrix} w_{0,\mathbf{k}} \\ w_{1,\mathbf{k}} \end{pmatrix}, \quad (\text{B8})$$

for any holomorphic invertible matrix S_k .

Our strategy will be to assume diagonal boundary conditions (B8) and holomorphic S_k and seek a contradiction. The boundary conditions of $v_{m\mathbf{k}}$ that we computed above, phrased in matrix notation, are

$$\begin{pmatrix} v_{0,\mathbf{k}+G} \\ v_{1,\mathbf{k}+G} \end{pmatrix} = e^{-i\mathbf{G}\cdot\mathbf{r}}\xi_{\mathbf{G}}(k) \begin{pmatrix} 1 & 0 \\ iB_0^{-1}\overline{G} & 1 \end{pmatrix} \begin{pmatrix} v_{0,\mathbf{k}} \\ v_{1,\mathbf{k}} \end{pmatrix}. \quad (\text{B9})$$

The boundary conditions for $w_{\mathbf{k}}$ are then related to the gauge transformation S_k as

$$S_{k+G} \begin{pmatrix} \tilde{\xi}_{\mathbf{G}}^{(0)}(k) & 0 \\ 0 & \tilde{\xi}_{\mathbf{G}}^{(1)}(k) \end{pmatrix} = \xi_{\mathbf{G}}(k) \begin{pmatrix} 1 & 0 \\ i\overline{G} & 1 \end{pmatrix} S_k. \quad (\text{B10})$$

We first focus on the top left entry of (B10), which reads

$$S_{00}(k+G)\tilde{\xi}_{\mathbf{G}}^{(0)}(k) = S_{00}(k)\xi_{\mathbf{G}}(k), \quad (\text{B11})$$

where S_{00} is the top left entry of S . Without loss of generality assume that the Chern number C_0 of the band described by $w^{0,\mathbf{k}}$ is zero or one (the Chern numbers must sum to two, and the Chern numbers of vortexable bands are positive). If $C_0 = 0$, then the band admits a tight-binding description with one delta-function-localized Wannier state per unit cell [20] and thus a gauge with $w_{0,\mathbf{k}} = 1$, and $\tilde{\xi}_{\mathbf{G}}^{(0)}(k) = 1$. Since S_k is invertible, we can demand that $h(k) = \partial_k \log S_{00}(k)$ is holomorphic. However, by (B11), with $\tilde{\xi}_{\mathbf{G}}^{(0)}(k) = 1$, we have $h(k+G) = h(k) + \frac{1}{2}\overline{G}$, so that by Lemma 1 $h(k)$ is not holomorphic. We therefore rule out the $C_0 = 0$ case, and focus on $C_0 = 1$.

Vortexable bands with $C_0 = 1$ have been classified [19, 88], and have boundary conditions $\tilde{\xi}_{\mathbf{G}}^{(0)}(k) = \eta_{\mathbf{G}}e^{\frac{1}{2}B^{-1}\overline{G}(k-k_0+\frac{G}{2})} = \xi_{\mathbf{G}}(k-k_0)$, for some offset k_0 . Then, Lemma 1 applied to $\log S_{00}(k)$ this time implies

$k_0 = 0$, so that $S_{00}(k+G) = S_{00}(k)$ is periodic. Periodic holomorphic functions are constant, so we can set $S_{00}(k) = 1$ without loss of generality. The lower-left component of (B10) then yields $S_{10}(k+G) = S_{10}(k) + iB_0^{-1}\bar{G}$, which again leads to a contradiction by Lemma 1. We have thus proven (P3), so that we can conclude that the trial wavefunctions used in the main text are first vortexable.

Appendix C: QGT of "maximal" first vortexability

In this section, we compute the quantum geometric tensor of the combined space of a "maximal" first vortexable band and its zeroth counterpart. By maximal, we specifically mean that there is no zeroth Landau level portion in the wavefunction other than what is required for the orthogonal basis. For example, in the language of the holomorphic periodic states of the previous section,

$$\begin{aligned} v_{kl}^{(0)} &= f_k(\mathbf{r})\mathcal{N}_0(\mathbf{r}), \\ v_{kl}^{(1)} &= 2i\partial_k f_k(\mathbf{r})\mathcal{N}_0(\mathbf{r}) + f_k(\mathbf{r})\mathcal{N}_1(\mathbf{r}), \end{aligned} \quad (\text{C1})$$

we demand $\mathcal{N}_1(\mathbf{r}) \rightarrow 0$. This corresponds to the limit $\gamma_1 \ell_B/v \rightarrow \infty$ in the Bernal graphene based Hamiltonians in the main text. In an orthonormal basis we then obtain

$$\begin{aligned} u_{0,\mathbf{k}} &= \frac{1}{N_{0,\mathbf{k}}} f_k(\mathbf{r})\mathcal{N}_0(\mathbf{r}), \\ u_{1,\mathbf{k}} &= \frac{1}{N_{1,\mathbf{k}}} Q_0(\mathbf{k})\partial_k u_{0,\mathbf{k}} \end{aligned} \quad (\text{C2})$$

where $Q_0(\mathbf{k}) = 1 - |u_{0,\mathbf{k}}\rangle\langle u_{0,\mathbf{k}}|$ orthogonalizes $u_{1,\mathbf{k}}$ relative to $u_{0,\mathbf{k}}$ and the factors $N_{m,\mathbf{k}}$ are such that the wavefunctions are normalized.

We recall property (V4), which states that vortexability of the bands is equivalent to $\hat{\eta}_{ab}^{\mu\nu} = \frac{1}{2}\hat{\Omega}_{ab}(\delta_{\mu\nu} - i\varepsilon_{\mu\nu})$, where the Berry curvature is

$$\hat{\Omega}_{ab}(\mathbf{k}) = \langle \partial_k u_{kb} | Q(\mathbf{k}) | \partial_k u_{ka} \rangle \quad (\text{C3})$$

We now show that $\hat{\Omega}_{00} = \hat{\Omega}_{01} = \hat{\Omega}_{10} = 0$, in the maximal $\mathcal{N}^{(1)} \rightarrow 0$ limit, so that the only nonzero entry is $\hat{\Omega}_{11}$, as claimed in the main text.

From (C3), it suffices to show $Q(\mathbf{k})|\partial_k u_{0,\mathbf{k}}\rangle = 0$. This in turn follows from writing

$$\begin{aligned} |\partial_k u_{0,\mathbf{k}}\rangle &= P_0 |\partial_k u_{0,\mathbf{k}}\rangle + Q_0 |\partial_k u_{0,\mathbf{k}}\rangle, \\ &= P_0 |\partial_k u_{0,\mathbf{k}}\rangle + N_{1,\mathbf{k}} |u_{1,\mathbf{k}}\rangle, \end{aligned} \quad (\text{C4})$$

where we used (C2). The first term is proportional to $u_{0,\mathbf{k}}$ by construction while the second term is proportional to $u_{1,\mathbf{k}}$, so that $Q(\mathbf{k})|\partial_k u_{0,\mathbf{k}}\rangle = 0$ as claimed.

Appendix D: γ_1 dependence for $M(\mathbf{k})$

In this section, we compute the "maximality index" which measures how close one is to the "maximal"

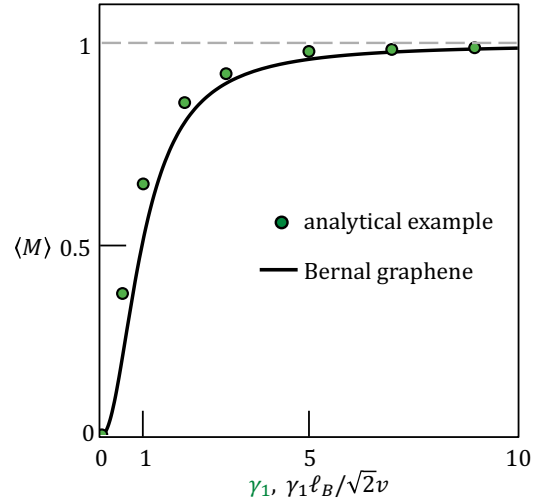


FIG. 4. $\langle M \rangle_{\text{BZ}}$ for the analytical example [Eq.(8)] (green points) and Bernal graphene with magnetic field [Eq.(2)] (black line) as a function of γ_1 , and $\gamma_1 \ell_B/\sqrt{2}v$, respectively.

first LL:

$$M(\mathbf{k}) = \frac{|\lambda_1(\mathbf{k}) - \lambda_2(\mathbf{k})|}{\lambda_1(\mathbf{k}) + \lambda_2(\mathbf{k})}, \quad (\text{D1})$$

where $\lambda_{1,2}$ are the eigenvalues of the 2×2 non-Abelian Berry curvature. The previous subsection implies $M(\mathbf{k}) = 1$ when $\mathcal{N}_1 \rightarrow 0$. Here we will compute M for Bernal graphene with constant $B > 0$ [Eq.(2)] analytically. We will also discuss the $M(\mathbf{k})$ of the chiral TBG example, which ends up closely related.

Bernal graphene in an external magnetic field has a continuous magnetic translation symmetry; the magnetic translation operators are $T(\mathbf{l}) = e^{-i\xi\mathbf{l}(\mathbf{r})}t(\mathbf{l})$ where $t(\mathbf{l}) = e^{i\mathbf{l}\cdot\nabla}$ is the ordinary, $B = 0$ translation operator. The phase satisfies $\mathbf{A}(\mathbf{r} + \mathbf{l}) = \mathbf{A}(\mathbf{r}) + \nabla\xi\mathbf{l}(\mathbf{r})$, where \mathbf{A} is the vector potential. The magnetic translation operators satisfy

$$T(\mathbf{l}_1)T(\mathbf{l}_2) = T(\mathbf{l}_2)T(\mathbf{l}_1)e^{iB\hat{z}\cdot\mathbf{l}_1 \times \mathbf{l}_2} \quad (\text{D2})$$

A commuting subset, generated by $T_{\mathbf{R}_1}, T_{\mathbf{R}_2}$ with $B\hat{z}\cdot\mathbf{R}_1 \times \mathbf{R}_2 = 2\pi$, can then be used to define Bloch states $\Phi_{\mathbf{k}}(\mathbf{r})$. The algebra (D2) implies that magnetic translations at other $\ell \neq \mathbf{R}$ act as "ladder operators" on the Bloch states, $T_{\ell}\Phi_{\mathbf{k}} \propto \Phi_{\mathbf{k}-B\hat{z}\times\ell}$ (see e.g. Appendix B of Ref. [88] for a pedagogical discussion). Thus, all Bloch momenta are symmetry related. We will shortly use this fact to specialize to calculating the Berry curvature at $\mathbf{k} = 0$.

The periodic states $\mathcal{U}_{m,\mathbf{k}} = e^{-i\mathbf{k}\cdot\mathbf{r}}\Phi_{m,\mathbf{k}}(\mathbf{r})$ of Bernal graphene have the form

$$\begin{aligned} \mathcal{U}_{0,\mathbf{k}} &= \begin{pmatrix} u_{0,\mathbf{k}} \\ 0 \end{pmatrix}, \\ \mathcal{U}_{1,\mathbf{k}} &= \frac{1}{\sqrt{\gamma_1^2 + 2(v\ell_B^{-1})^2}} \begin{pmatrix} \gamma_1 u_{1,\mathbf{k}} \\ \sqrt{2}v\ell_B^{-1}u_{0,\mathbf{k}} \end{pmatrix} \end{aligned} \quad (\text{D3})$$

where $u_{0\mathbf{k}}$ is the periodic state of the usual LLL and $u_{1,\mathbf{k}}$ is that of the usual first LL, obtained from the lowest through the raising operator. Both states are normalized. We will shortly use

$$u_{1,\mathbf{k}} = \sqrt{B}Q_0(\mathbf{k})\partial_k u_{0,\mathbf{k}} \quad (\text{D4})$$

which can be computed directly or indirectly. The indirect route begins by writing $u_{1,\mathbf{k}} = \lambda Q_0(\mathbf{k})\partial_k u_{0,\mathbf{k}}$. One then solves for $\lambda = \sqrt{B}$ through $1 = \langle u_{1,\mathbf{k}} | u_{1,\mathbf{k}} \rangle = |\lambda|^2 \langle \partial_k u_{0,\mathbf{k}} | Q_0(\mathbf{k}) | \partial_k u_{0,\mathbf{k}} \rangle = |\lambda|^2 \Omega_{\text{LLL}}$, where we have identified $\Omega_{\text{LLL}} = 1/B$ as the Berry curvature of the LLL. We will also use

$$\begin{aligned} \langle u_{1,\mathbf{k}} | \partial_k u_{0,\mathbf{k}} \rangle &= \sqrt{B} \langle \partial_k u_{0,\mathbf{k}} | Q_0(\mathbf{k}) | \partial_k u_{0,\mathbf{k}} \rangle, \\ &= \sqrt{B} \Omega_{\text{LLL}} = 1/\sqrt{B}. \end{aligned} \quad (\text{D5})$$

We are now ready to compute the non-Abelian Berry curvature

$$\hat{\Omega}_{mn}(\mathbf{k}) = \langle \partial_k \mathcal{U}_{n,\mathbf{k}} | Q(\mathbf{k}) | \partial_k \mathcal{U}_{m,\mathbf{k}} \rangle. \quad (\text{D6})$$

Let us fix $\mathbf{k} = 0$ without loss of generality, so that we can more easily apply rotation symmetry (recall that all momenta are related by magnetic translation symmetry, such that $\hat{\Omega}$ is \mathbf{k} -independent). We note that $\mathcal{U}_{1,\mathbf{k}=0}$ has a different angular momentum than $\mathcal{U}_{0,\mathbf{k}=0}$. This implies that the off-diagonal elements of $\hat{\Omega}$ must vanish.

The diagonal terms follow from

$$\begin{aligned} \hat{\Omega}_{00} &= \langle \partial_k \mathcal{U}_{0,\mathbf{k}} | (1 - P_0 - P_1) | \partial_k \mathcal{U}_{0,\mathbf{k}} \rangle \\ &= \langle \partial_k \mathcal{U}_{0,\mathbf{k}} | Q_0 | \partial_k \mathcal{U}_{0,\mathbf{k}} \rangle - \langle \partial_k \mathcal{U}_{0,\mathbf{k}} | P_1 | \partial_k \mathcal{U}_{0,\mathbf{k}} \rangle \\ &= \Omega_{\text{LLL}} - \frac{\gamma_1^2}{\gamma_1^2 + 2(v\ell_B^{-1})^2} |\langle u_{1,\mathbf{k}} | \partial_k u_{0,\mathbf{k}} \rangle|^2 \\ &= B^{-1} \frac{2(v\ell_B^{-1})^2}{\gamma_1^2 + 2(v\ell_B^{-1})^2}. \end{aligned} \quad (\text{D7})$$

Because the trace of the non-Abelian Berry curvature must be $2/B$, to be consistent with $C = 2$ for the two-band system, we must have

$$\hat{\Omega}_{11} = B^{-1} \frac{2(v\ell_B^{-1})^2 + 2\gamma_1^2}{\gamma_1^2 + 2(v\ell_B^{-1})^2}. \quad (\text{D8})$$

We therefore obtain

$$M = \frac{\gamma_1^2}{\gamma_1^2 + 2(v\ell_B^{-1})^2}, \quad (\text{D9})$$

as claimed in the main text. At $\gamma_1 \rightarrow 0$ which corresponds to the decoupling of Bernal graphene into two identical monolayer graphene, the ingredients of non-Abelian Berry curvature are $\hat{\Omega}_{01} = \hat{\Omega}_{10} = 0$ and $\hat{\Omega}_{00} = \hat{\Omega}_{11} = 1/B$ so the maximal index is $M = 0$. On the other hand, at $\gamma_1 \rightarrow \infty$, $\hat{\Omega}_{00} = \hat{\Omega}_{01} = \hat{\Omega}_{10} = 0$ and $\hat{\Omega}_{11} = 2/B$, leading to $M = 1$.

We numerically calculate the $\langle M(\mathbf{k}) \rangle_{\text{BZ}}$ for the analytical example [Eq.(8)] at magic angle $\alpha = 0.586$ in Fig.4. The index depends on γ_1 almost as same as that of Bernal graphene $B > 0$.

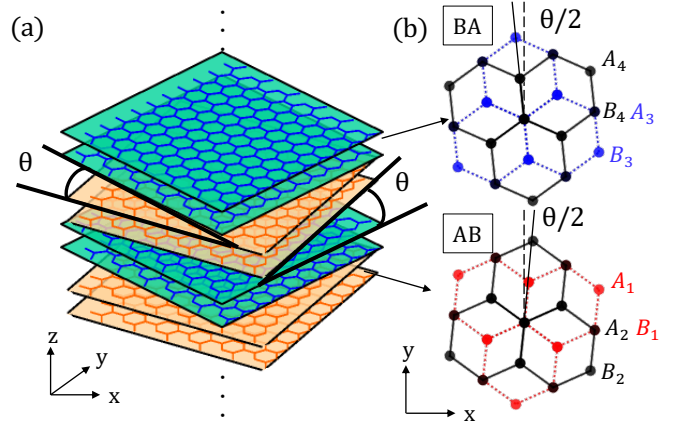


FIG. 5. Schematic picture of three-dimensional alternatively ABBA twisted Bernal graphene.

Appendix E: Three dimensional twisted AB-BA double bilayer

The Hamiltonian [Eq.(8)] corresponds to the model where the layers are twisted by $(0, \theta, \theta, 2\theta)$ and hosts a hopping between different sublattices of the next nearest layers. Using the unitary transformation such as changing the order of layer basis $(|\sigma, 1\rangle, |\sigma, 2\rangle, |\sigma, 3\rangle, |\sigma, 4\rangle)$ into $(|\sigma, 1\rangle, |\sigma, 3\rangle, |\sigma, 4\rangle, |\sigma, 2\rangle)$, where $\sigma = \pm$ denotes A/B, we obtain the following Hamiltonian

$$\mathcal{H}_{3\text{DATDBG}} = \mathcal{H}_{\text{AB-BA}} + \begin{pmatrix} 0 & 0 & 0 & T^\dagger(\mathbf{r}) \\ 0 & 0 & 0 & 0 \\ 0 & 0 & 0 & 0 \\ T(\mathbf{r}) & 0 & 0 & 0 \end{pmatrix}. \quad (\text{E1})$$

where the first term is the Hamiltonian of twisted AB-BA double bilayer (TDBG) [89]

$$\mathcal{H}_{\text{AB-BA}} = \begin{pmatrix} -i\sigma \cdot \nabla & \Gamma_1^\dagger & 0 & 0 \\ \Gamma_1 & -i\sigma \cdot \nabla & T^\dagger(\mathbf{r}) & 0 \\ 0 & T(\mathbf{r}) & -i\sigma \cdot \nabla & \Gamma_1 \\ 0 & 0 & \Gamma_1^\dagger & -i\sigma \cdot \nabla \end{pmatrix} \quad (\text{E2})$$

with $\Gamma_1 = (\sigma_x - i\sigma_y)\gamma_1/2$.

$$T(\mathbf{r}) = \sum_{n=1}^3 T_n e^{-i\mathbf{q}_n \cdot \mathbf{r}} \quad (\text{E3})$$

where $T_{n+1} = \alpha(\sigma_x \cos n\phi + \sigma_y \sin n\phi)$ is the interlayer hopping in the chiral limit. The second term is the interlayer coupling between layer 1 and 4, implying imposing the periodic boundary condition to the twisted AB-BA double bilayer in the stacking direction. This model can be realized in three-dimensional alternatively twisted AB-BA double bilayer graphene shown in Fig. 5. In an infinite number of stackings of TDBG, the wavenumber k_z along the stacking direction is a good quantum number to label the energy state. At $k_z = 0$, the Hamiltonian is equivalent to Eq.(E1).